A simple post-processing method to correct species predictions in artificially thickened turbulent flames

Pascal Gruhlke, Eray Inanc, Renaud Mercier, Benoit Fiorina, Andreas M Kempf

A simple post-processing method to correct species predictions in artificially thickened turbulent flames

Pascal Gruhlke, Eray Inanc, Renaud Mercier, Benoit Fiorina, Andreas Kempf

A simple post-processing method to correct species predictions in artificially thickened turbulent flames

Pascal Gruhlke [a,*], Eray Inanc [a], Renaud Mercier [b], Benoît Fiorina [c], Andreas M. Kempf [a]

[a] *Chair of Fluid Dynamics, Institute for Combustion and Gas Dynamics (IVG), University of Duisburg-Essen, Germany*
[b] *Safran Tech, Modelling & Simulation, Rue des Jeunes Bois, Châteaufort, Magny-Les-Hameaux 78114, France*
[c] *Laboratoire EM2C, CNRS, CentraleSupélec, Université Paris-Saclay, 3 rue Joliot Curie, Gif Sur Yvette cedex 91192, France*

Abstract

An efficient method for accurate species (such as CO) concentration predictions on artificially thickened flames is proposed and demonstrated for the Cambridge swirled flame. This method relies on corrections of the (side-) effects introduced by the (dynamic) flame thickening and wrinkling models, applied as an LES post-processing step. This technique provides better predictions of minor species in the inner reaction zone wherever a thickened flame model is used – provided that the flame burns in the flamelet regime, and that the interest is on in-flame data rather than on post-flame data. A demonstration for CO concentrations is given and compared to experimental evidence. It is concluded that the thickening factor correction is universal and can be applied for all species, whereas the efficiency factor correction must be adjusted for each species, and heat loss level separately. Both corrections were found to reduce the grid and code dependencies of the results. As this technique is easy to understand, easy to implement and suitable as a correction for available data, we recommend its use in all applications of thickened flame models.

Keywords: Large-Eddy simulation; Species prediction; Stratified flames; Artificially Thickened Flames (ATF); Thickened Flame Model for LES (TFLES)

1. Introduction

Thanks to its ability to handle unsteady phenomena, Large-Eddy Simulation (LES) of turbulent flames is a key tool for predicting pollutant emissions from industrial combustors [1]. To account for the complex chemical pathways involved, LES has been combined with various chemistry modelling strategies. Despite of recent impressive demonstrations [2–5], the prediction of pollutant formations, especially of CO, remains a major challenge for combustion LES.

A first issue is caused by the artificial broadening of the flame front, which is required because the
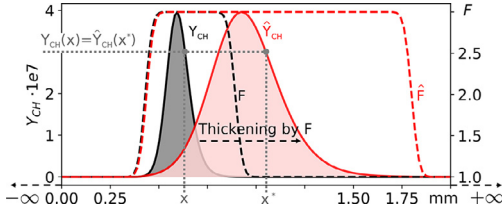
Fig. 1. Impact of the flame thickening by intermediate species (CH) mass fraction with $F_{max} = 3$. Black lines: non-thickened quantities φ. Red line: thickened quantities $\hat{\varphi}$. Thickening increases the total amount of the species (illustrated by the gray area) to a much greater amount (illustrated by the transparent red area). (For interpretation of the references to color in this figure legend, the reader is referred to the web version of this article.)

laminar flame thickness is normally smaller than the mesh size [6]. Among the possible solutions, the thickened flame model for LES (TFLES) [7], or artificially thickened flame model (ATF) [8], is a pragmatic and popular approach. It modifies the diffusive and reactive terms of the species balance equation, to artificially thicken the flame while preserving the laminar flame speed. This approach is straightforward to implement and has been used in combination with tabulated or direct chemistry by many authors [9,10]. The species profiles are however thickened, as illustrated by the shaded areas in Fig. 1, so that the total mass of the species found within the computational domain is increased. Overpredictions of the CO peak values in the flame brush have been attributed to flame thickening in recent simulations [11,12].

A second issue is the impact of the subgrid flame wrinkling patterns on the species production. Moureau et al. [13] observed that subgrid-scale quantities (like species) are also influenced by the surface of the flame contained at the subfilter scale. Mercier et al. [14] proposed a correction based on manufactured filtered wrinkled flamelets to account for the impact of subgrid-scale flame wrinkling for the species production. The correction has been implemented in the filtered flame formalism (F-TACLES) but was never attempted for the thickened flame (TFLES/ATF) framework.

This article proposes a post-processing correction, straightforward to implement, for improving the prediction of minor species obtained from thickened flame models applied to LES. The method is valid for premixed and weakly stratified turbulent flames burning in the flamelet regime.

2. Combustion modeling

Flame thickening is obtained by multiplying diffusion terms and dividing chemical reaction rates by a thickening factor F. Unfortunately, this broadening process also reduces the wrinkling of the species mass fractions iso-surfaces, the flame surface area and hence the turbulent flame speed. This reduction of the turbulent flame-speed is compensated by an efficiency function or subgrid-scale wrinkling factor Ξ. The resulting equation for a thickened species mass fraction $\hat{Y}_k$ reads:

$$\frac{\partial \bar{\rho} \hat{Y}_k}{\partial t} + \frac{\partial}{\partial x_i} \left(\bar{\rho} \tilde{u}_i \hat{Y}_k \right)$$
$$= \frac{\partial}{\partial x_i} \left(\left[F \Xi \frac{\mu}{Sc} + (1 - \Omega) \frac{\mu_t}{Sc_t} \right] \frac{\partial \hat{Y}_k}{\partial x_i} \right) + \frac{\Xi}{F} \dot{\omega}_k \quad (1)$$

Eq. (1) depends on density ρ, viscosity μ, turbulent viscosity μ_t, Schmidt number Sc, turbulent Schmidt number Sc_t and source term $\dot{\omega}_k$ of species k. To avoid increased diffusive fluxes in non reacting regions, a dynamic formulation of the thickening factor F is applied, $F = 1 + (F_{max} - 1)\Omega$, with a maximum thickening factor F_{max}. The flame sensor Ω is defined as 0 (respectively 1) outside (respectively inside) the reaction layer.

2.1. Laminar flame thickening correction

Theoretical framework

The laminar profile of a typical intermediate species mass fraction $Y_{CH}(x)$ is sketched in Fig. 1 over the spatial coordinate x normal to the flame front, where $x \to -\infty$ and $x \to +\infty$ correspond to fresh and burnt gases, respectively. Each element dx of this flame is artificially thickened in x-direction by the thickening factor $F(x)$, which is continuous, greater or equal to 1 and defined on $\mathbb{R}$. The thickened spatial coordinate is then defined as:

$$x^* = \int_0^x F(x)dx = f(x) \quad (2)$$

The anti-derivative f is bijective and differentiable. Any thickened variable $\hat{\varphi}$ therefore reads:

$$\hat{\varphi}(x^*) = \varphi(x) = \varphi\left(f^{-1}(x^*)\right) \quad (3)$$

As discussed in the introduction, the thickening operator does not conserve the total mass $\mathcal{M}_k = \int_{-\infty}^{+\infty} \rho(x)Y_k(x)dx$ of the kth species. Indeed, the total mass of the species in the thickened flame reads in the thickened spatial dimension x^*:

$$\hat{\mathcal{M}}_k = \int_{-\infty}^{+\infty} \hat{\rho}(x^*)\hat{Y}_k(x^*)dx^* \quad (4)$$

Eq. (4) can be rewritten using Eq. (3):

$$\hat{\mathcal{M}}_k = \int_{-\infty}^{+\infty} \rho\left(f^{-1}(x^*)\right) Y_k\left(f^{-1}(x^*)\right)dx^* \quad (5)$$

As f is differentiable on $\mathbb{R}$, Eq. (5) can be integrated by substitution of $x^* = f(x)$ in the original spatial dimension x:
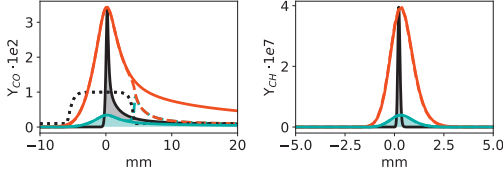
Fig. 2. Laminar 1-D premixed flame solution. Laminar, thickened and corrected thickened flames profiles of CO (left) and CH (right) mass fractions for a constant thickening factor $F = 10$. Black solid lines: Y_k (laminar). Red solid lines: $\hat{Y}_k$ (thickened). Turquoise lines: $\hat{Y}_k^c$ (thickened and corrected). The dotted lines show a (scaled) dynamic thickening factor function. (For interpretation of the references to color in this figure legend, the reader is referred to the web version of this article.)

$$\hat{\mathcal{M}}_k = \int_{-\infty}^{+\infty} \rho(x) Y_k(x) \frac{df}{dx} dx \qquad (6)$$

$$= \int_{-\infty}^{+\infty} F(x) \rho(x) Y_k(x) dx \neq \mathcal{M}_k \qquad (7)$$

Eq. (7) shows that flame thickening will bias the total mass of species contained in the computational domain by F(x). To compensate this error, an *a posteriori* corrected species mass fraction is defined as:

$$\hat{Y}_k^c(x^*) = \hat{Y}_k(x^*) / \hat{F}(x^*) \qquad (8)$$

With this correction, the total mass of the species is well retrieved. Indeed, the corrected integral of the species mass fraction reads:

$$\hat{\mathcal{M}}_k^c = \int_{-\infty}^{+\infty} \hat{\rho}(x^*) \hat{Y}_k^c(x^*) dx^* \qquad (9)$$

$$= \int_{-\infty}^{+\infty} \hat{\rho}(x^*) \hat{Y}_k(x^*) / \hat{F}(x^*) dx^* = \mathcal{M}_k \qquad (10)$$

This leads to a simple and effective strategy for compensating the error introduced by flame thickening at the time when LES samples are taken: the corrected species mass is obtained if each sample taken from the thickened flame is divided by the local thickening factor of the thickened flame $\hat{F}(x)$, following Eq. (8).

This strategy is illustrated in Fig. 2, which shows mass fraction profiles from a CH_4-air laminar premixed flame at $\Phi = 0.83$ computed with GRI-3.0 [15]. The CH profile is representative of an intermediate species, which exists only in the reaction zone. The CO species exhibits a more complex profile with a peak in the reaction zone but a non-zero value in the burnt products. For the sake of clarity, thickened flame profiles are shown for a constant flame sensor $\Omega = 1$ and a thickening factor $F = 10$. The figure illustrates how the artificial flame thickening causes an increase of the total mass of species contained within the flame front. The plot also shows the corrected mass fraction

profiles $\hat{Y}_k^c$, as introduced in Eq. (8), conserving the total mass of species.

To summarise, correct time averages of species mass fractions are only available from LES if each sample is divided by the local thickening factor at the time of sampling. In other words, mean species concentrations should no longer be computed by Reynolds averaging as $<\hat{Y}_k(x^*)>$, but rather as:

$$<\hat{Y}_k^c(x^*)> = <\hat{Y}_k(x^*) / \hat{F}(x^*)> \qquad (11)$$

The laminar flame thickening correction is based only on the resolved chemical flame structure. Its implementation does not dependent of the kinetics models used and can be combined either with tabulated or transported chemistry. Changing an LES code for this corrected sampling is straightforward but must be done while individual samples are available.

Post-processing of mean laminar flame brush

The impact of the correction on time-averaged profiles is first tested with a planar flame front (flamelet). A mean flame brush is generated assuming a uniform spatial distribution of flamelet positions [16]. This procedure mimics turbulence-flame interactions in flamelet regimes where the flame wrinkling is fully resolved. The distribution is $L = 20$ mm wide, centred at $x^* = 0$ and obtained from $5 \cdot 10^5$ equally spaced flame positions. The flame brush width L is representative of the flame thickness in the downstream region of the Cambridge flame [17], retained here to validate the thickened flame correction. The number of flame positions is selected to ensure statistical convergence.

Thin black lines in Fig. 3 show examples of the distributed unsteady laminar profiles. The Reynolds averaging of this flamelet ensemble provides the reference mean mass fraction $< Y_k >$ shown by the black bold line in Fig. 3 for CH, CO and CO_2. The same procedure is applied on a thickened laminar profile distribution, illustrated by thin red lines in Fig. 3. The mean of the thickened flame profiles $<\hat{Y}_k>$, shown by the bold red lines, dramatically overestimates the mean reference solution.

In turn, the mean corrected mass fractions calculated as $<\hat{Y}_k^c(x^*)>=<\hat{Y}_k(x^*)/\hat{F}(x^*)>$ improve the quality of the prediction significantly, in particular for the averaged corrected CH profiles which perfectly match the reference solution. In general, the correction is very efficient in reconstructing the mean profiles of intermediate species, but bigger deviations remain in CO species. The problem is largely caused by the constant thickening factor that does not revert to unity for $x \to \pm\infty$, with species concentrations that do not revert to zero for $x \to \pm\infty$. The problem can be overcome if a dynamic thickening factor is used, as illustrated by the dashed turquoise line in Fig. 3, achieving a much-improved mean species mass fraction.
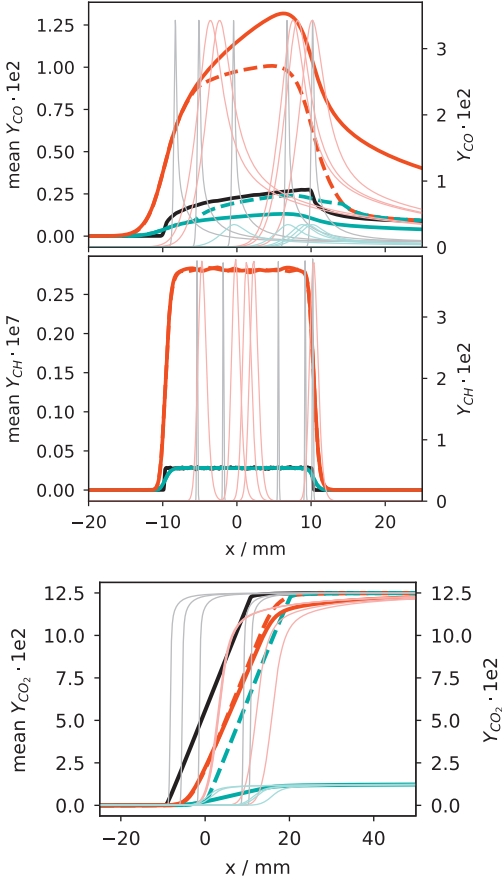
Fig. 3. Bold lines: Reynolds time-averaged profiles of CO (top), CH (middle) and CO_2 (bottom) mass fractions generated to mimic a turbulent flame brush. Black lines: $<Y_k>$ (laminar). Red lines: $<\hat{Y}_k>$ (thickened). Turquoise lines: $<\hat{Y}_k^c>$ (thickened and corrected). Thin dotted lines: some of the randomly distributed flamelet solutions of CO (top) and CH (bottom) mass fractions. Dashed lines show results of dynamic thickening, solid lines for constant thickening (F=10). (For interpretation of the references to color in this figure legend, the reader is referred to the web version of this article.)

The thickened and corrected profiles of the CO_2 mass fractions show that results are consistent only with dynamic thickening as the factor must revert to one away from the flame. Even in that case, unlike to CH and CO profiles, the correction does not improve the prediction. This observation applies to all major species that exhibit a monotonic evolution across the flame front such as reactants or main products.

Note that, when the flame thickening factor approaches the size of the flame brush, unsteady effects are attenuated and the mean flame solution becomes similar to laminar profiles shown in Fig. 2.
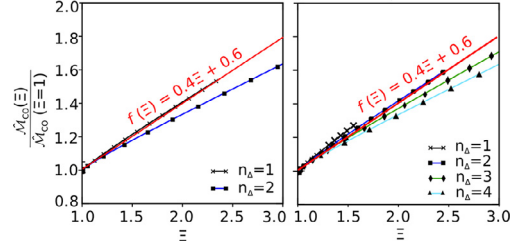

Fig. 4. Normalized mass of CO in term of subgrid-scale flame wrinkling Ξ at a filter size $\Delta = 5\delta_l^0$ (left) and $\Delta = 10\delta_l^0$ (right), where δ_l^0 is the laminar flame thickness. Results are plotted for different numbers of flame patterns n_Δ. Extracted from [14].

2.2. Turbulent flame wrinkling factor correction

In turbulent flames, thickened quantities are also influenced by the flame wrinkling pattern at the sub-grid scale. For the flamelet regime, the impact of the unresolved flame wrinkling on the species prediction has been modelled [14] with filtered wrinkled flamelets (FWF): two-dimensional wrinkled flamelets are generated from detailed chemistry, freely propagating, laminar premixed flame solutions, by assuming that the reactive layers follow sinusoidal patterns. A FWF is characterized by the filter width Δ, wrinkling factor Ξ and the number of sinusoidal periods n_Δ within a filter width. The mass of any species k is then determined from integrating over the FWF elements.

As an example, a series of FWF elements has been computed for a premixed CH_4-air mixture at a given equivalence ratio of 0.83 with GRI-3.0. The mass m_{CO}^T of CO contained at the subgrid-scale Δ is plotted in Fig. 4 in terms of the flame wrinkling factor Ξ for different flame patterns n_Δ.

To ease the interpretation, m_{CO}^T is normalized by m_{CO}^L, the mass of CO in laminar flames. Results show that i) the ratio m_{CO}^T/m_{CO}^L increases almost linearly with flame wrinkling because of the increased flame surface, and that ii) the mass of CO is relatively independent of n_Δ. From these observations, the following relation is proposed for correcting the thickened species mass fractions:

$$\hat{Y}_k^{c,T}(x^*) = \hat{Y}_k^T(x^*)(a\Xi + b) \qquad (12)$$

The model constants a and b can be estimated from FWF elements. Fig. 4 shows that a good estimation of these constants is $a = 0.4$ and $b = 0.6$ (red curve). It is also worth noting that this estimation is valid for a large range of filter widths Δ and thickening factors F. In case of very large filter widths, the correction factor equals the wrinkling factor ($a = 1$, $b = 0$) but only for totally intermediate species (i.e. only in the flame front). This is true for CH but not for CO, as already discussed by Mercier et al. [14].

3. Experimental and numerical setup

The Cambridge burner [17] consists of an outer tube ($D = 34.8$ mm), an inner tube ($D = 23.6$ mm) and a coaxial cylindrical bluff body, acting as a flame holder. The burner is embedded in a co-flow of air. The swirled case SwB3 with a low level of stratification has been studied, with inner and outer streams at 8.3 m/s and 18.7 m/s mean velocities and an equivalence ratio of 0.75. Experimental results are available for velocity, temperature and species mass fractions [17,18].

Highly resolved low-Mach simulations with homogeneous and isotropic cartesian grids were performed with the in-house code PsiPhi [9,19–21]. The convective fluxes of scalars were interpolated using a TVD-scheme, momentum by central differencing. The unresolved fluxes in momentum and scalars were estimated from an eddy viscosity ν_t determined by Nicoud's σ-model [22]. The subgrid contributions of the Favre-filtered mixture fraction and progress variable were estimated based on the work by Floyd et al. [23]. The simulations were performed in a $(180 \text{ mm})^3$ domain made of 38 million cells with a uniform grid spacing of 0.5 mm. A further simulation with a resolution of 0.25 mm in a $(250 \text{ mm})^3$ domain with one billion cells was performed to confirm grid and domain independence and to test the need for the correction on a very fine mesh.

Simulations were also performed with the compressible OpenFOAM on unstructured grids. TVD schemes were used for scalars and momentum, time was advanced with a non-central Crank-Nicholson scheme with weights of 0.41 (explicit) and 0.59 (implicit). The sub-grid viscosity was computed with a transported sub-grid kinetic energy model [24]; a uniform sub-grid distribution was assumed for scalars. A domain of $(180 \text{ mm})^3$ was discretised by an unstructured grid, resolving 0.5 mm in the flame region, with a total of 17 million cells.

A commonly made unity Lewis assumption was used by both codes and combustion chemistry was modelled by the FPI/FGM approach [25,26]. One-dimensional adiabatic freely propagating laminar flame computations with GRI-3.0 were mapped to a look-up table parameterized by the mixture fraction Y_z and a progress variable defined as $Y_c = Y_{CO_2} + Y_{H_2O} + Y_{CO}$. Within the thickened flame formalism, balance equations for the thickened progress variable $\hat{Y}_c$ and mixture fraction $\tilde{Y}_z$ were solved.

Both PsiPhi and OpenFOAM simulations used a dynamic thickened flame approach [27] with the flame sensor $\Omega = 16[\tilde{c}(\tilde{c} - 1)]^2$ [28]. The upper cut-off scale was $n\Delta_X$ as suggested by Colin et al. [7], where Δ_X was the cell size and $n = 5$ was chosen as proposed by Charlette et al. [29] and tested by Proch et al. [30]. The wrinkling factor Ξ was estimated based on the Charlette model [29] with a static constant of $\beta = 0.5$. A power-law veloc-

Table 1
Conducted simulations.

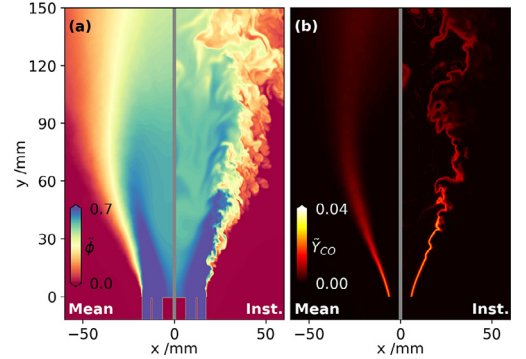| Solver	PsiPhi	PsiPhi	OpenFoam
#cells	47 M	1000 M	17 M
Δ_X/mm	0.5	0.25	0.5
F_{max}	5	2.5	5
time/s	1.0	1.0	1.0
size/mm^3	180^3	250^3	180^3
#CPU	1728	27,000	1272
CPUh	0.05 M	1.3 M	0.3 M

Fig. 5. Mean (left sub-figure) and instantaneous (right sub-figure) equivalence ratio $\tilde{\phi}$ (a) and CO mass fraction $\tilde{Y}_{CO}$ (b) in a section through the centre-line.

ity profile was imposed at the inlet, superimposed with synthetic turbulence [31,32] in both PsiPhi and OpenFOAM. All simulations were performed under adiabatic conditions. A summary of the simulated cases is given in Table 1.

4. Results and testing

Figure 5 illustrates the flame, showing mean and instantaneous equivalence ratio and CO mass fractions.

Three post-processing procedures are applied to the results of LES simulations indicated in Table 1: i) uncorrected Reynolds time averaging of thermo chemical quantities resulting in $<\hat{Y}_k>$, ii) Reynolds averaging with the laminar correction of Eq. (11) yielding $<\hat{Y}_k^c>$ and iii) Reynolds averaging with the turbulence correction from Eq. (12), which results in $<\hat{Y}_k^{c,T}>$. As chemistry is modeled by the FPI/FGM approach, instantaneous thickened species mass fractions are obtained from the chemical look-up table as $\hat{Y}_k = \hat{Y}_k(\hat{Y}_c, \tilde{Y}_z)$.

For a quantitative comparison of simulations and experimental data, we refer to the supplementary material, to other work from our group [9] and to Figs. 6–10, which show both the effect of the correction and the agreement with the experiments.

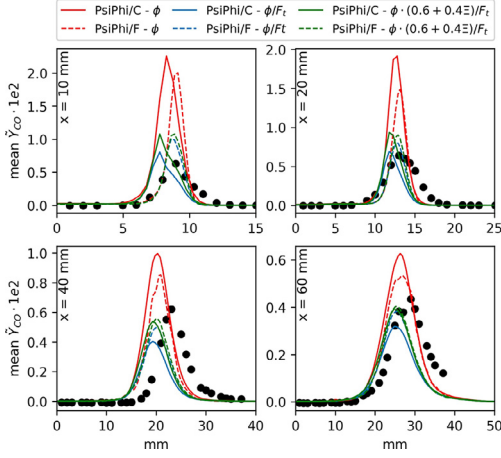Fig. 6 shows the mean CO mass fraction as a function of the radius at four axial locations using

Fig. 6. Radial mean mass fraction of *CO* at several locations above the burner for coarse and fine PsiPhi simulations. Red lines: uncorrected $<\hat{Y}_{CO}>$. Blue lines: with laminar correction $<\hat{Y}_{CO}^{c}>$. Green lines: with turbulent correction $<\hat{Y}_{CO}^{c,T}>$. Dashed lines: fine grid. Solid lines: coarse grid. (For interpretation of the references to color in this figure legend, the reader is referred to the web version of this article.)

Fig. 7. Integration of the mean mass fraction of *CO* at several location above the burner for coarse and fine PsiPhi simulations in radial direction. Red lines: uncorrected $<\hat{Y}_{CO}>$. Blue lines: with laminar correction $<\hat{Y}_{CO}^{c}>$. Green lines: with turbulent correction $<\hat{Y}_{CO}^{c,T}>$. Dashed lines: fine grid. Solid lines: coarse grid. (For interpretation of the references to color in this figure legend, the reader is referred to the web version of this article.)
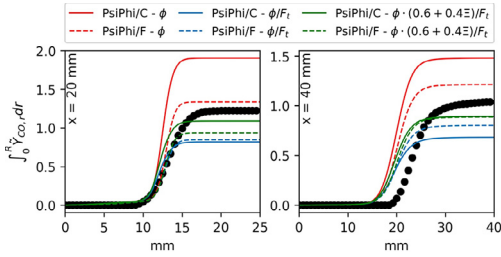
PsiPhi and a coarse (0.5 mm) and a fine (0.25 mm) grid. Post processed LES solutions are shown by red lines for $<\hat{Y}_{k}>$, blue lines for $<\hat{Y}_{k}^{c}>$ and green lines for $<\hat{Y}_{k}^{c,T}>$. At all axial locations, it is obvious how the weighting lowers the excessive peak concentrations of CO to more reasonable values – correcting the total mass of the species contained in this region. It is worth noting that even a simulation with a rather fine grid (0.25 mm, one billion cells) will benefit from the proposed correction. At the downstream locations (40–60 mm), pure weighting with the thickening factor leads to low CO values, which are enhanced again by the additional consideration of the wrinkling factor. At the upstream
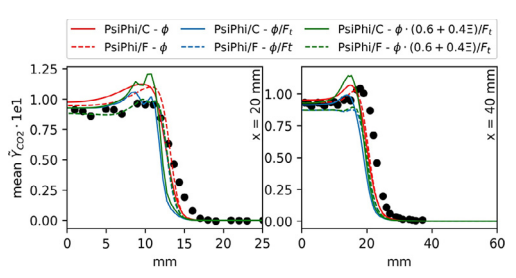

Fig. 8. Radial mean mass fraction of CO_2 at several location above the burner for coarse and fine PsiPhi simulations. Red lines: uncorrected $<\hat{Y}_{CO_2}>$. Blue lines: with laminar correction $<\hat{Y}_{CO_2}^{c}>$. Green lines: with turbulent correction $<\hat{Y}_{CO_2}^{c,T}>$. Dashed lines: fine grid. Solid lines: coarse grid. (For interpretation of the references to color in this figure legend, the reader is referred to the web version of this article.)

Fig. 9. Radial mean mass fraction of *CO* at several location above the burner for coarse simulations. Red lines: uncorrected $<\hat{Y}_{CO}>$. Blue lines: with laminar correction $<\hat{Y}_{CO}^{c}>$. Green lines: with turbulent correction $<\hat{Y}_{CO}^{c,T}>$. Dashed lines: OpenFOAM. Solid lines: PsiPhi (coarse grid). (For interpretation of the references to color in this figure legend, the reader is referred to the web version of this article.)
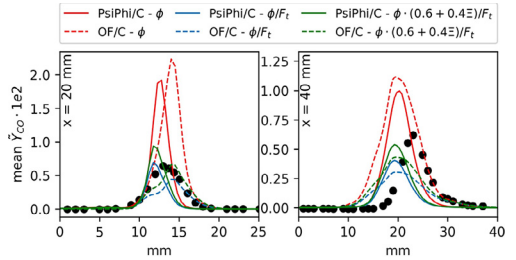

Fig. 10. Integration of the mean mass fraction of *CO* at several location above the burner on the radial direction for coarse simulations. Red lines: uncorrected $<\hat{Y}_{CO}>$. Blue lines: with laminar correction $<\hat{Y}_{CO}^{c}>$. Green lines: with turbulent correction $<\hat{Y}_{CO}^{c,T}>$. Dashed lines: OpenFOAM. Solid lines: PsiPhi (coarse grid). (For interpretation of the references to color in this figure legend, the reader is referred to the web version of this article.)
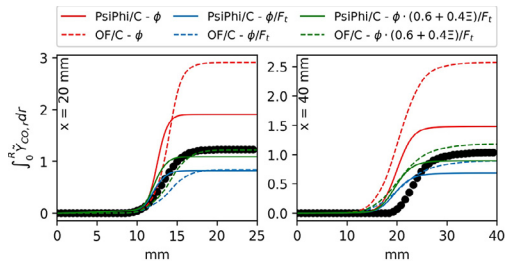
locations (20 mm to 30 mm), it seems that considering the impact of subgrid-scale flame wrinkling leads to slightly high CO peaks, but the integral values are still improved. Overall, it's worth noting that the effect of the wrinkling factor correction is stronger downstream since the flame is hardly wrinkled near the burner and only becomes corrugated further downstream [9].

It was mentioned before that the accurate CO prediction could be considered in an integral sense. One could then argue that the integral of the CO mass fraction along a radial line should agree between experiments and simulations – irrespective of local deviations. In other words: a wider peak should go in hand with a lower peak value. This integral of the CO mass fraction over the radius is shown in Fig. 7 for both grids. It is quite apparent how the simple averaging (red) leads to excessive values, but also how the results improve with grid refinement, as expected. Applying the weighting with the thickening factor only (blue) lowers the integral values by an excessive amount and the additional correction with the efficiency function is needed to achieve the best result (green). Even more striking is by which degree the grid dependency is reduced by the weighting with the thickening factor: where the original integral (red) changes with the grid by up to 50%, the weighted integral (blue) changes only up to 10% – providing evidence that an inherent grid effect has been removed.

Both laminar and turbulent corrections are mainly relevant for species mass fraction fields sensitive to the LES filter properties or flame thickening. This concerns intermediates like CH and products with non-monotonic behavior like CO. Fig. 8 shows that, as for laminar regimes, the corrections does not significantly improve CO_2. The average flame location (where CO_2 mass fractions drop off) is nevertheless shifted a little towards the centre-line, as a result of the "removed" flame thickening. Near the centre-line, the mass-fraction drops off by a small amount only, as even the thickened flame will almost never reach this region. It must be stressed that a poor result would be obtained here if a constant thickening factor is used instead of the dynamic one.

Finally, the comparison between the in-house code PsiPhi and the common OpenFOAM software is shown; for the CO mean mass fractions and its radial integrals, in Figs. 9 and 10. These results confirm the previous findings and show how well the proposed weighting and correction for the thickening factor and the efficiency function work. From the integral plot in Fig. 10, it is also apparent that after weighting and correction, the results agree far better between the two codes and grids - reducing not only errors but also sensitivity. Much of the original deviations are probably explained by the different local grid resolutions, LES models and numerical schemes used by the two codes.

5. Conclusions

To conclude, the consideration of the thickening factor and efficiency function in the LES-post processing seems to be an easy, effective way for obtaining more accurate averaged mass fractions of in flame species wherever a thickened flame model is used – provided that the flame burns in a flamelet regime, that the interest is on in-flame data rather than on post-flame data, and that a dynamic thickening factor is used. It is, however, worth noting that only the laminar thickening factor weighting is universal and can be applied for all species, whereas the turbulent wrinkling factor correction must be adjusted for each species or heat loss level separately. Further testing the effect of changing coefficients for the turbulent correction will be conducted in future work. The post-processing has been successfully applied here within a tabulated chemistry context. This is not restrictive as the methodology and the conclusion would be identical within another formalism such as reduced or detailed chemistry.

It is also apparent that after weighting and correction, the results agree far better between the two codes and the grids – reducing not only errors but also sensitivity. To conclude, we have demonstrated an effective method to predict accurate species concentrations, which is also simple to implement and to apply.

Declaration of Competing Interest

None.

Acknowledgments

References

[1] B. Fiorina, D. Veynante, S. Candel, *Flow Turb. Combust.* 94 (1) (2015) 3–42.

[2] B. Wegner, U. Gruschka, W. Krebs, Y. Egorov, H. Forkel, J. Ferreira, K. Aschmoneit, *J. Eng. Gas Turb. Power* 133 (7) (2011-07-01) 71502(7).

[3] G. Bulat, W.P. Jones, A.J. Marquis, *Combust. Flame* 161 (7) (2014) 1804–1825.

[4] T. Jaravel, E. Riber, B. Cuenot, G. Bulat, *Proc. Combust. Inst.* 35 (3) (2016) 3817–3825.

[5] P. Gruhlke, E.I. Mahiques, S. Dederichs, F. Proch, C. Beck, A.M. Kempf, *J. Eng. Gas Turb. Power* 140 (10) (2018) 101502.

[6] T. Poinsot, D. Veynante, *Theoretical and Numerical Combustion*, RT Edwards, France, 2005. p. 472

[7] O. Colin, F. Ducros, D. Veynante, T. Poinsot, *Phys. Fluids A* 12 (7) (2000) 1843–1863.

[8] G. Kuenne, F. Seffrin, F. Fuest, T. Stahler, A. Ketelheun, D. Geyer, J. Janicka, A. Dreizler, *Combust. Flame* 159 (8) (2012) 2669–2689.

[9] F. Proch, P. Domingo, L. Vervisch, A.M. Kempf, *Combust. Flame* 180 (2017) 321–339.

[10] W. Han, H. Wang, G. Kuenne, E.R. Hawkes, J.H. Chen, J. Janicka, C. Hasse, *Proc. Combust. Inst.* 37 (2) (2019) 2555–2563.

[11] G. Maio, M. Cailler, R. Mercier, B. Fiorina, *Proc. Combust. Inst.* 37 (2) (2019) 2591–2599.

[12] P. Benard, G. Lartigue, V. Moureau, R. Mercier, *Proc. Combust. Inst.* 37 (4) (2019) 5233–5243.

[13] V. Moureau, P. Domingo, L. Vervisch, *Combust. Flame* 158 (7) (2011) 1340–1357.

[14] R. Mercier, C. Mehl, B. Fiorina, V. Moureau, *Combust. Flame* 205 (2019) 93–108.

[15] G.P. Smith, et al., Gri-Mech 3.0, combustion. berkeley.edu/gri-mech, 2000.

[16] L. Vervisch, P. Domingo, G. Lodato, D. Veynante, *Combust. Flame* 157 (4) (2010) 778–789.

[17] M.S. Sweeney, S. Hochgreb, M.J. Dunn, R.S. Barlow, *Combust. Flame* 159 (9) (2012) 2896–2911.

[18] M.S. Sweeney, S. Hochgreb, M.J. Dunn, R.S. Barlow, *Combust. Flame* 159 (9) (2012) 2912–2929.

[19] A.M. Kempf, B.J. Geurts, J.C. Oefelein, *Combust. Flame* 158 (12) (2011) 2408–2419.

[20] E. Inanc, M.T. Nguyen, S. Kaiser, A.M. Kempf, *Comp. Fluids* 140 (2016) 435–449.

[21] E. Inanc, A.M. Kempf, *Fuel* 252 (2019) 408–416.

[22] F. Nicoud, H.B. Toda, O. Cabrit, S. Bose, J. Lee, *Phys. Fluids* 23 (8) (2011) 085106.

[23] J. Floyd, A.M. Kempf, A. Kronenburg, R.H. Ram, *Combust. Theor. Model.* 13 (4) (2009) 559–588.

[24] A. Yoshizawa, K. Horiuti, *J. Phys. Soc. Jpn.* 54 (8) (1985) 2834–2839.

[25] O. Gicquel, N. Darabiha, D. Thévenin, *Proc. Combust. Inst.* 28 (2) (2000) 1901–1908.

[26] J.A. van Oijen, L.P.H. de Goey, *Combust. Sci. Technol.* 161 (1) (2000) 113–137.

[27] J.P. Legier, T.J. Poinsot, D. Veynante, *Proc. Summer Prog.* (2000) 157–168.

[28] L. Durand, W. Polifke, *ASME Turbo Expo* (2007) 869–878.

[29] F. Charlette, C. Meneveau, D. Veynante, *Combust. Flame* 131 (2002) 159–180.

[30] F. Proch, A.M. Kempf, *Combust. Flame* 161 (10) (2014) 2627–2646.

[31] M. Klein, A. Sadiki, J. Janicka, *J. Comput. Phys.* 186 (2) (2003) 652–665.

[32] A.M. Kempf, M. Klein, J. Janicka, *Flow, Turb. Comb.* 74 (1) (2005) 67–84.